Supplementary Information

S1 Materials and methods

S1.1 Chemicals and reagents

All 89 selected pharmaceutical standards were of analytical grade with purity > 98% (see Table S1 for the name and structure of the pharmaceuticals). Internal standards (IS) were used as reported by (Grabic et al., 2012) by addition of the following: $^{2}H_{6}$–codeine, $^{2}H_{4}$–diclofenac, $^{2}H_{4}$–flecainide, $^{2}H_{3}$–ketoprofen, $^{13}C_{3}{}^{2}H_{3}$–naproxen, and $^{13}C_{3}$–paracetamol, all from CDN-Isotopes (pointe-Claire, Quebec, Canada). LC/MS grade methanol and acetonitrile were purchased from Merk (Lichrosoiv-hypergrade, Merck, Darmstadt, Germany). Formic acid for the mobile phases (0.1% v/v) (Lindberg et al., 2014) and sodium thiosulfate were purchased from Sigma-Aldrich (Steinheim, Germany). Na_2SO_4 was analytical grade and purchased from Beijing Chemical Works Co., China. Pharmaceutical stock solutions were prepared by dissolving the standards in methanol, evaporating the methanol, then re-dissolving them in Milli-Q water (resistivity > 18 MΩ).

Table S1 Pharmaceuticals used in the empirical analyses and modeling in this study, their classes, level of quantification (LOQ), and molecular structures

Compound	Class	LOQ (ng/L)	Molecular structure
Alfuzosin	Urological	4	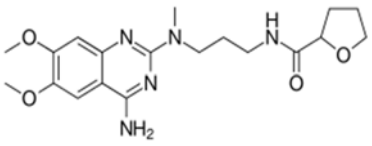
Alprazolam	Psycholeptic	20	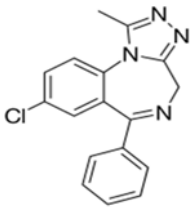
Amitriptyline	Antidepressant	10	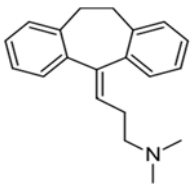
[a]Atenolol	Hypertension drug	15	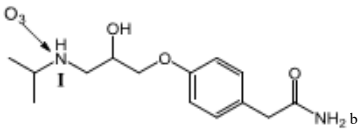

Atorvastatin	Statin	10	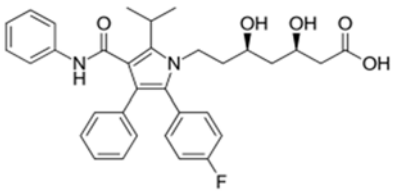
Atracurium	Muscle relaxant	4	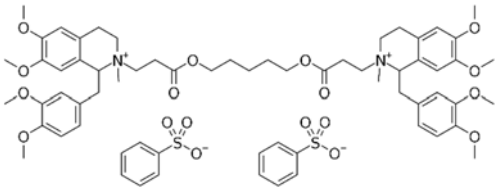
Azelastine	Anti-histamine	2	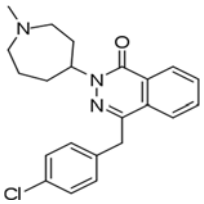
[a]Azithromycin	Antibiotic	40	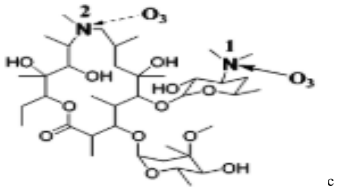
Beclomethasone	Anti-inflammatory corticoid	80	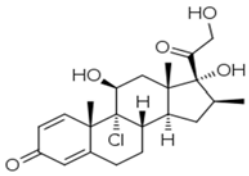
Biperiden	Anti-Parkinson	3	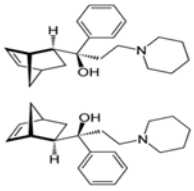
Bisoprolol	Hypertension drug	3	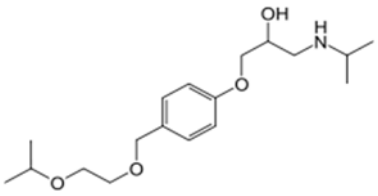
Bromocriptine	Anti-Parkinson	15	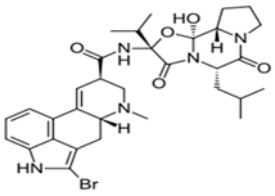

Budesonide	Anti-inflammatory corticoid	20	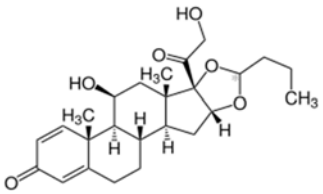
Buprenorphine	Analgesic	20	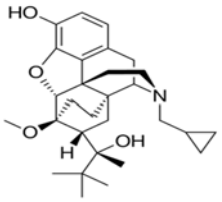
Bupropion	Antidepressant	3	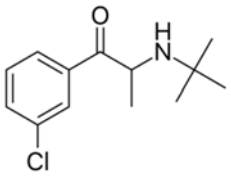
[a]Caffeine	Psycholeptic	20	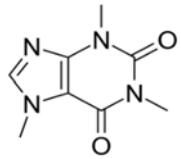
[a]Carbamazepine	Antiepileptic	7.5	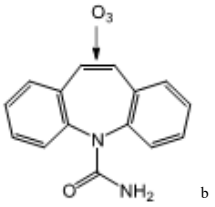 b
Cilazapril	Hypertension drug	2	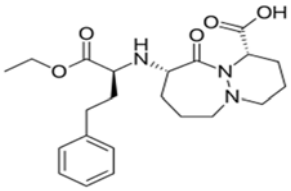
[a]Ciprofloxacin	Antibiotic	10	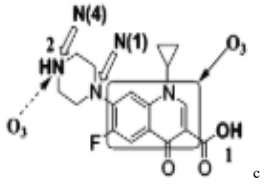 c
Citalopram	Antidepressant	15	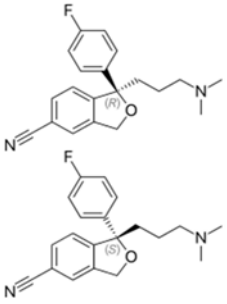

[a]Clarithromycin	Antibiotic	3	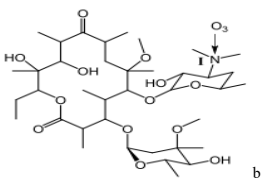 b
Clemastine	Antidepressant	2	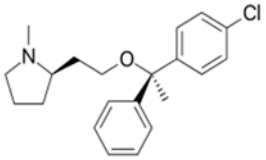
[a]Clindamycin	Antibiotic	3	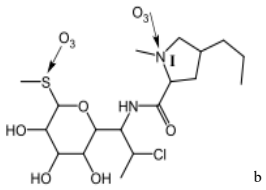 b
Clomipramine	Antidepressant	2	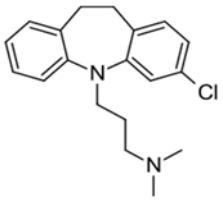
Clonazepam	Psycholeptic	10	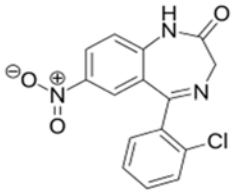
Clotrimazol	Antimycotic	10	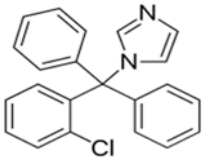
Codeine	Analgesic	15	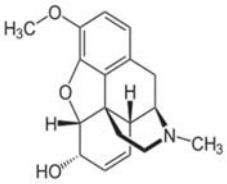
Cyproheptadine	Antihistamine	7.5	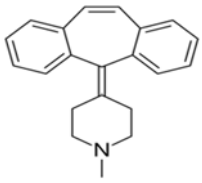
Desloratadine	Antihistamine	15	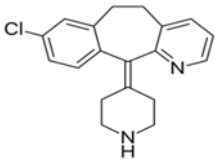

[a]Diclofenac	Nonsteroid anti-inflammatory drug	10	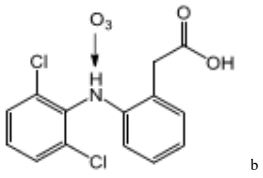 [b]
Dicycloverine	Gastrointestinal disorder drug	10	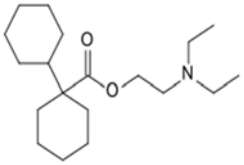
Dihydroergotamine	Analgesic	15	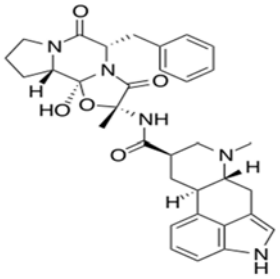
Diltiazem	Hypertension drug	2	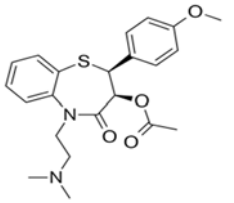
Diphenhydramine	Antihistamine	4	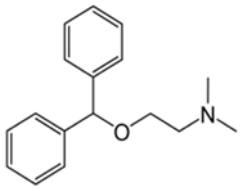
Dipyridamole	Antithrombotic agent	3	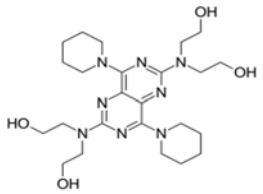
Donepezil	Anti-Alzheimer	7.5	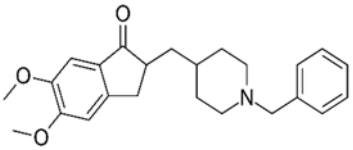
Duloxetine	Antidepressant	2	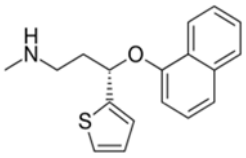

[a]Eprosartan	Hypertension	15	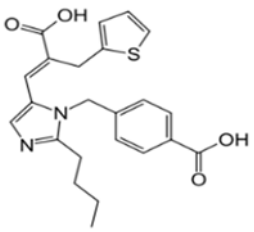
[a]Erythromycin	Antibiotic	20	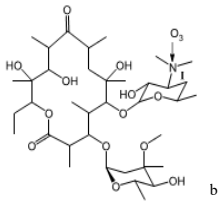 b
[a]Fexofenadine	Antihistamine	10	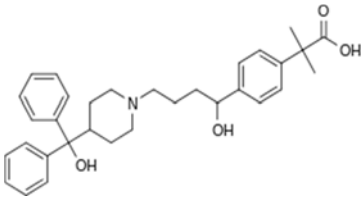
Finasteride	Urological	20	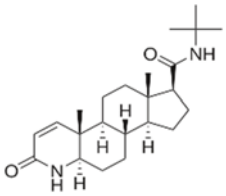
Flecainide	Antiarrhythmic	2	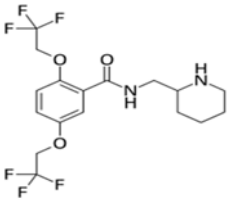
[a]Fluconazole	Antimycotic	7.5	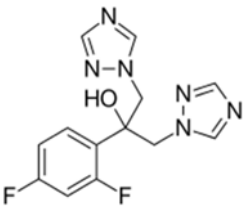
Flunitrazepam	Psycholeptic	10	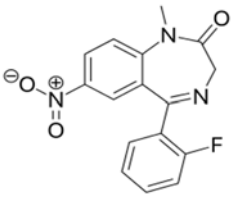
[a]Fluoxetine	Antidepressant	7.5	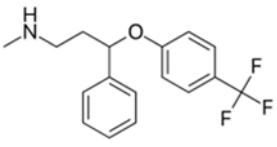

Flupentixol	Psycholeptic	10	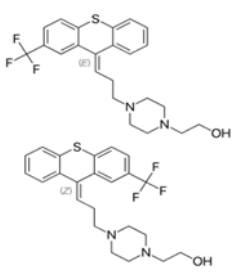
Fluphenazine	Psycholeptic	10	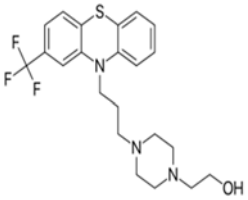
Glibenclamide	Antidiabetic	20	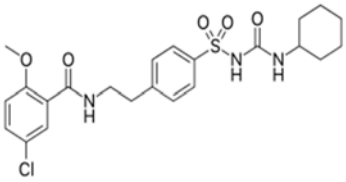
Glimepiride	Antidiabetic	20	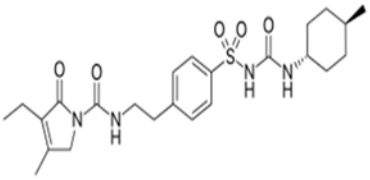
Haloperidol	Psycholeptic	3	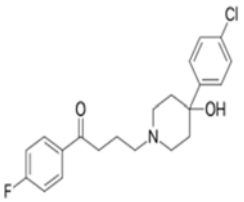
Hydroxyzine	Psycholeptic	3	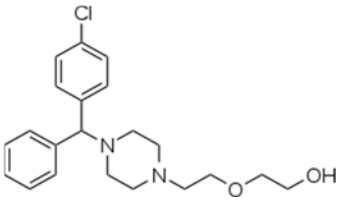
[a]Irbesartan	Hypertension drug	3	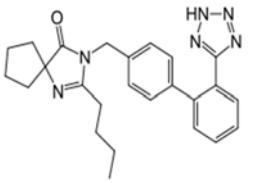
Levomepromazine	Psycholeptic	20	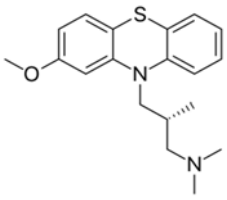

Loperamide	Antipropulsive	2	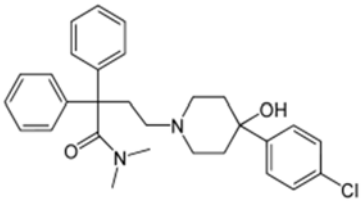
Maprotiline	Antidepressant	15	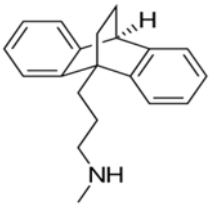
Memantine	Psycholeptic	3	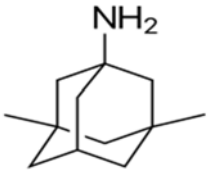
[a]Metoprolol	Hypertension drug beta blocking agent	15	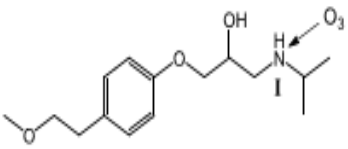 [b]
Mianserin	Antidepressant	3	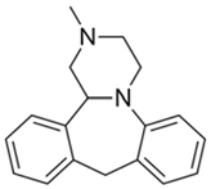
Mirtazapine	Antidepressant	15	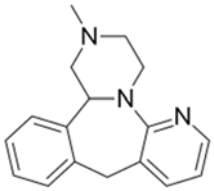
Naloxone	Opoid overdose drug Narcotic antagonist	2	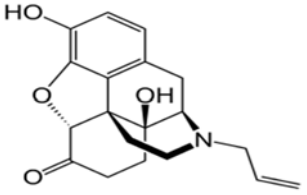 Phenol [b]
Nefazodone	Antidepressant	2	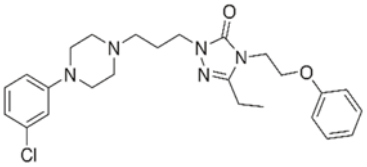

[a]Norfloxacin	Antibiotic	20	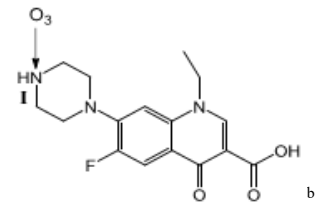 [b]
[a]Ofloxacin	Antibiotic	3	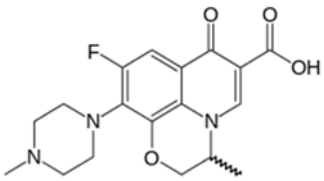
Orphenadrine	Antihistamine	3	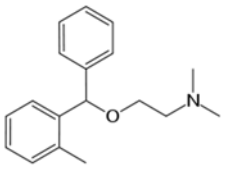
[a]Oxazepam	Psycholeptic	10	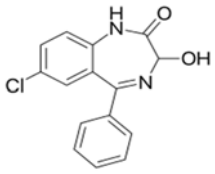
Oxytetracycline	Antibiotic	10	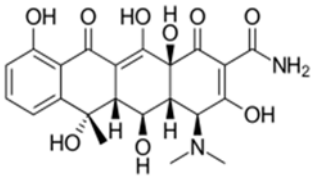
[a]Paracetamol	Analgesic	30	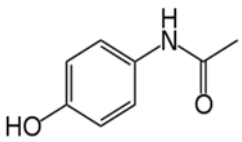
Paroxetine	Antidepressant	10	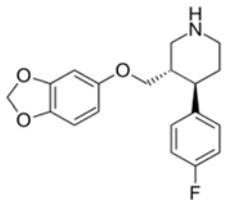
Perphenazine	Psycholeptic	20	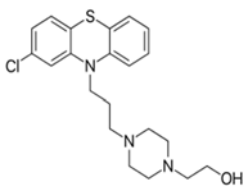

Pizotifen	Analgesic	2	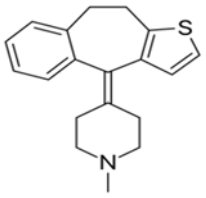	
Promethazine	Neuroleptic	15	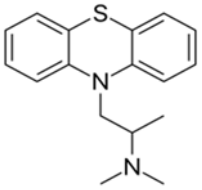	
[a]Propranolol	Beta blocking agent	20	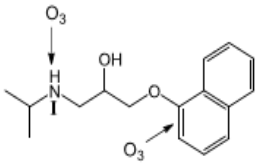	Amine/benzene [b]
[a]Ranitidine	Peptic ulcer drug	20	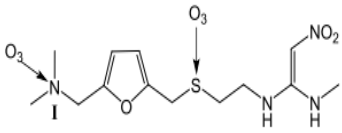	
Repaglinide	Antidiabetic	2	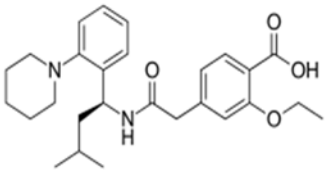	
Risperidone	Psycholeptic	4	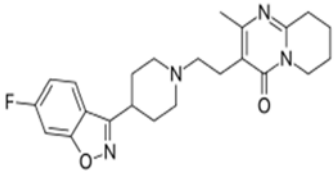	
Rosuvastatin	Statin	20	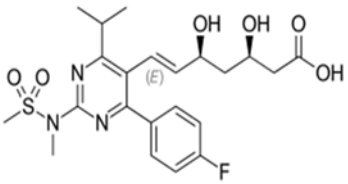	
[a]Roxithromycin	Antibiotic	15	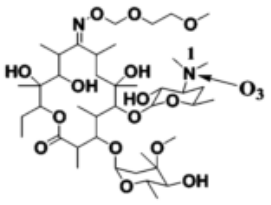	

Sertraline	Antidepressant	10	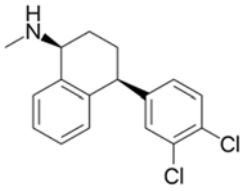
[a]Sotalol	Hypertension drug	15	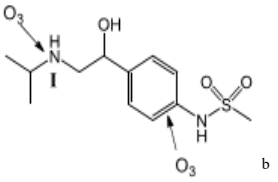 b
[a]Sulfamethoxazole	Antibiotic	15	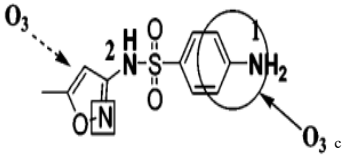 c
[a]Telmisartan	Hypertension drug	10	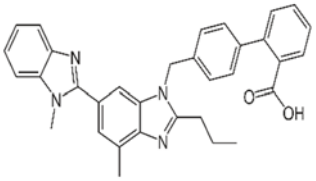
Terbutaline	Broncodilator	3	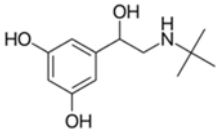
[a]Tetracycline	Antibiotic	20	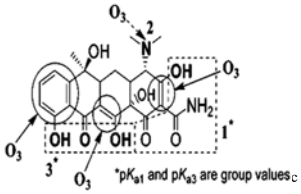 c
[a]Tramadol	Analgesic	15	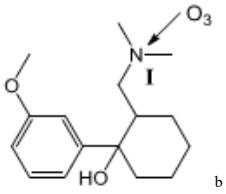 b
Trihexyphenidyl	Anti-Parkinson	3	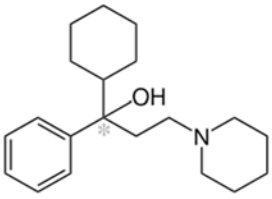

[a]Trimethoprim	Antibiotic	3	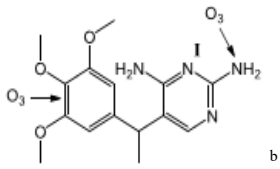 b
[a]Venlafaxine	Antidepressant	20	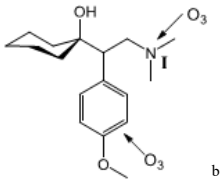 b
[a]Verapamil	Hypertension drug	10	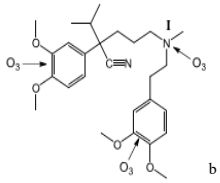 b
Zolpidem	Psycholeptic	3	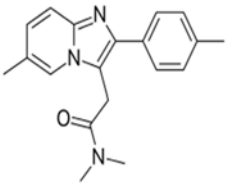

Notes: a) Pharmaceuticals used in QSAR model development; b) (Lee et al., 2014); c) (Dodd et al., 2006)

Table S2 Main water quality parameters of the secondary effluent used in this study

Constituent	Secondary effluent
pH	7.3
Dissolved organic carbon (DOC, mg/L)	8.40
HCO_3^- (mg/L)	244
Alkalinity (mg/L as $CaCO_3$)	201
Total dissolved solids (TDS, mg/L)	602
Turbidity (NTU)	0.19
Conductivity (μS/cm)	970
Ca^{2+} (mg/L)	80.6
Mg^{2+} (mg/L)	25.7
Na^+ (mg/L)	101
Cl^- (mg/L)	128
SO_4^{2-} (mg/L)	67.4
Ammonia (mg/L)	0.63
•OH scavenging rate from DOM [a] (s^{-1})	2.9×10^5
•OH scavenging rate from HCO_3^- [b] (s^{-1})	3.4×10^4
•OH scavenging rate from NH_4^+ [c] (s^{-1})	3.3×10^3
Total •OH scavenging rate (s^{-1})	3.3×10^5

Notes: a) $k_{\bullet OH/DOM} = 3.5 \times 10^4$ L/(mg C)/s (von Sonntag and von Gunten, 2012); b) $k_{\bullet OH/HCO_3^-} = 8.5 \times 10^6$ $M^{-1} \cdot s^{-1}$ (Buxton et al., 1988); c) $k_{\bullet OH/NH_4^+} = 9.0 \times 10^7$ $M^{-1} \cdot s^{-1}$ (Buxton et al., 1988)

The total •OH scavenging rate of the secondary effluent due to its background water constituents is calculated according to Eq. (S1).

$$k_{scav} = k_{\bullet OH,DOM}[DOM] + k_{\bullet OH,HCO_3^-}[HCO_3^-] + k_{\bullet OH,NH_4^+}[NH_4^+] \quad (S1)$$

When the water was spiked with pharmaceuticals (P_i), the scavenging rate of the spiked pharmaceuticals relative to the total scavenging rate can be calculated according to Eq. (S2).

$$\text{Contribution (\%)} = \frac{\sum_i k_{\bullet OH,P_i}[P_i]}{k_{\bullet OH,DOM}[DOM] + k_{\bullet OH,HCO_3^-}[HCO_3^-] + k_{\bullet OH,NH_4^+}[NH_4^+] + \sum_i k_{\bullet OH,P_i}[P_i]} \times 100 \quad (S2)$$

Based on the 35 out of spiked 89 pharmaceuticals with known $k_{\bullet OH}$, the scavenging rate of the 35 pharmaceuticals was calculated to be 8×10^2 s^{-1}. Thus, the scavenging rate of all the 89 pharmaceuticals was estimated to be 2×10^3 s^{-1}, which is less than 1% of that of the background water constituents. Due to their low concentrations, the spiked pharmaceuticals will not considerably change the ozone chemistry (e.g., O_3 decomposition and •OH scavenging) in the selected wastewater. Most of O_3 and •OH will be consumed in the reactions with background water constituents such as dissolved organic matter (DOM) and carbonate, while the spiked pharmaceuticals can only be oxidized in competition.

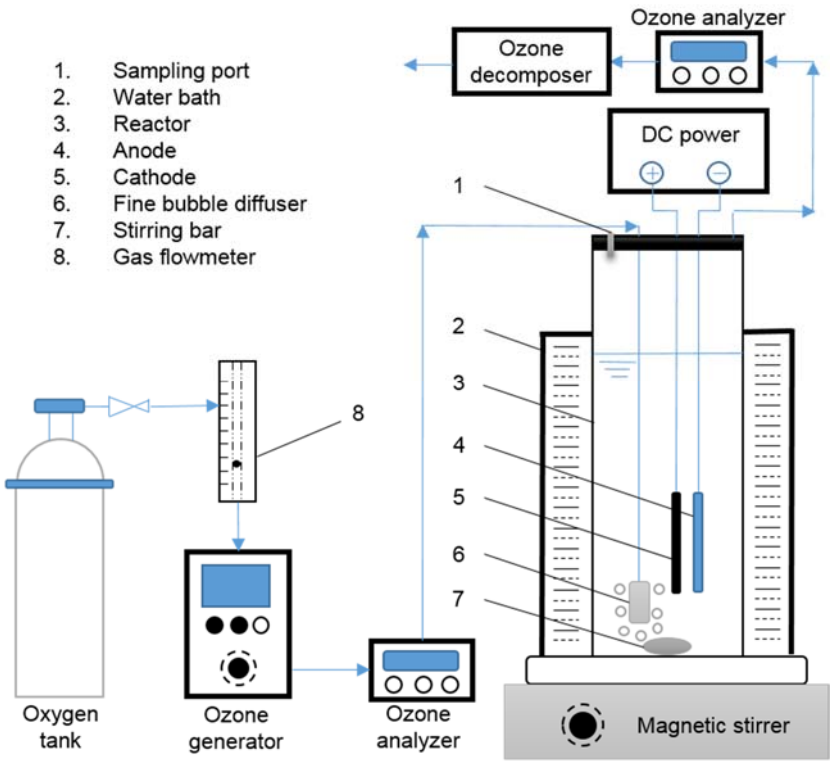

Fig. S1 Schematic of the reactor used for ozonation and the E-peroxone treatment

For the E-peroxone process, a platinum anode (2 × 2 cm^2) and carbon-polytetrafluoroethylene (carbon-PTFE) cathode (5 × 2 cm^2) were installed in the reactor. The carbon-PTFE electrode was prepared with Vulcan XC-72 carbon powder (Cabot Corp., USA), PTFE dispersion, and anhydrous alcohol according to the procedures described elsewhere (Wang et al., 2012).

All data were collected from duplicate experiments at each point to capture the variation in pharmaceuticals' responses to the treatments. Triplicate samples under initial conditions were collected. The variability was less than 30% at almost all data points, but higher than 30% at a few points, especially when the analytes' concentrations were close to the limit of quantitation (LOQ, defined as a signal to noise ratio of 10:1).

S1.2 Analytical methods

During each treatment, 10 mL samples were collected from the reactor at preset time intervals. O_3 and H_2O_2 concentrations were measured using the indigo method (Bader and Hoigne, 1981) and the potassium titanium (IV) oxalate method (Sellers, 1980), respectively. For pharmaceutical analysis, 200 µL of sodium thiosulfate (0.1 M) was immediately added to each sample to quench the residual oxidants. After adding 50 µL of IS mix to each sample (corresponding to 5 ng/IS/sample) to follow potential losses of pharmaceuticals during storage, samples were stored at 4℃ in the dark and analyzed within 4 weeks of collection. The pharmaceuticals were analyzed as previously reported (Grabic et al., 2012; Lindberg et al., 2014). Briefly, automated online solid phase extraction (SPE) was used in combination with liquid chromatography (LC) and triple stage quadrupole mass spectrometry (MS/MS). Samples were acidified to pH 3 using formic acid and 1 mL of the resulting solution was injected into the LC-MS/MS system (Thermo Fisher Scientific, San Jose, CA, USA) via a 1 mL loop. Injected samples were

then passed through an OASIS HLB (20 mm × 2.1 mm i.d., 15 µm particle size) online extraction column (Waters, Milford, Massachusetts, USA) followed by a guard column (20 mm × 2.1 mm i.d.) and an analytical column (50 mm × 2.1 mm i.d.). Both the guard and analytical columns were supplied by Thermo Fisher Scientific (San Jose, CA, USA) and contained 5 µm particles of Hypersil GOLD aQ C18 polar end-capped stationary phase. The analytes were ionized by heated electrospray ionization (HESI), in negative or positive ion mode. Vaporizer and capillary temperatures were 200℃ and 325℃, respectively, and the ionization voltage was 3.5 kV. Argon was used as the collision gas at a pressure of 1.5 mTorr and the resolution of the mass analyzing quadrupoles was 0.7 FMWH. Pharmaceuticals were quantified by internal standard calibration (ISC) (see Table S1 for the LOQs). The total time required for a complete analysis (online extraction and LC-MS/MS analysis of a sample) was approximately 15 min (see Table S3).

Table S3 LC analysis and mobile phase information

Analysis procedure	**Time (min)**	**H_2O (0.1% FA) %**	**ACN (0.1% FA) %**	**Flow mL/min**
Surveyor pump,	0	100	0	0.05
online solid	0.01	100	0	1.1
phase extraction	2	100	0	1.1
	2.01	0	100	0.3
	7	0	100	0.3
	7.01	100	0	1
	11	100	0	1
	11.01	100	0	0.05
Accela pump,	0	95	5	0.25
analytical LC	2	95	5	0.25
	5	75	25	0.35
	10	0	100	0.4
	12.99	0	100	0.4
	13	95	5	0.25
	15	95	5	0.25

Table S4 Additional pharmaceuticals used in QSAR model development, but not included in the experimental investigation

Compound	Class	Molecular structure	pk_a	k_{O3} [a] ($M^{-1}\cdot s^{-1}$)	$k_{\cdot OH}$ [b] ($M^{-1}\cdot s^{-1}$)
Bezafibrate	Lipid modifier	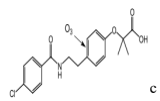 [c]	3.3 [e]	590 [c]	7.4×10^9 [f]
Ibuprofen	Nonsteroid anti-inflammatory drug	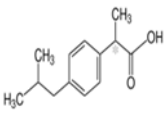	4.9 [e]	9.6 [f]	7.4×10^9 [f]
Valsartan	Hypertension drug	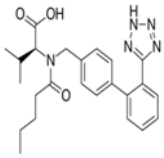	4.4, 7.4 [g]	38 [c]	$\sim 10^{10}$ [c]
Primidone	Anticonvulsant	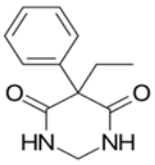	2.4, 3.9 [g]	1 [f]	9.1×10^9 [c]
Gabapentin	Antiepileptic	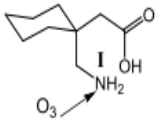 [c]	9.9 [c]	220 [c]	9.1×10^9 [c]
Lamotrigine	Antiepileptic	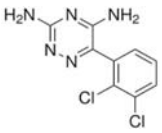	8.5 [g]	4 [h]	
Diazepam	Psycholeptic	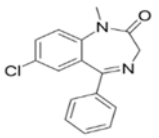	3.4 [i]	0.75 [f]	
Phenytoin	Antiepileptic	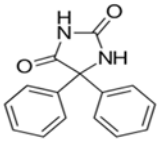		10 [j]	6.3×10^9 [k]
Meprobamate	Antianxiety	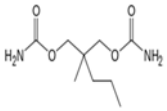		1 [j]	3.7×10^9 [l]
Levetiracetam	Antiepileptic	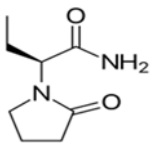		< 1 [c]	3.8×10^9 [c]

Candesartan	Hypertension drug	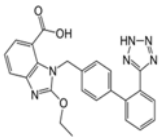		560 [m]
Metformin	Antidiabetic	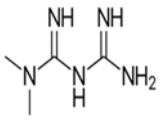	10.3 [n]	1.2 [n]
Progesterone	Hormone therapy	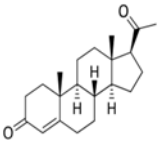		480 [l]
Azacyclonol	Antipsychotic	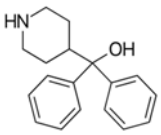		350 [o]
Medroxyprogesterone	Hormone therapy	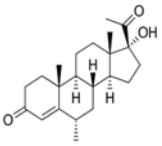		558 [p]

Notes: a) k_{O3} represents the apparent second-order rate constant of the indicated pharmaceutical with O_3 at pH 7 unless otherwise stated; b) $k_{\bullet OH}$ represents the apparent second-order rate constant of the indicated pharmaceutical with •OH at pH 7 unless otherwise stated; c) (Lee et al., 2014); d) (Dodd et al., 2006); e) (Rosal et al., 2008); f) (Huber et al., 2003); g) (Bourgin et al., 2017); h) (Keen et al., 2014); i) (Muñoz et al., 2008); j) (Lee et al., 2013); k) (Yuan et al., 2013); l) (Lee and von Gunten, 2012); m) (Bourgin et al., 2018); n) (Jin et al., 2012); o) (Borowska et al., 2016); p) (Broséus et al., 2009)

S2 Results and discussion

S2.1 Consumed O_3 dose and electro-generated H_2O_2 dose

During the E-peroxone process, an O_2/O_3 gas mixture was continuously sparged in the reactor, while H_2O_2 was electrochemically generated from O_2 reduction at the cathode. Consumed O_3 doses were calculated according to the gas phase O_3 concentrations at the reactor inlet and outlet as well as the aqueous O_3 concentrations during the treatment (see Figs. S2(a)–S2(c) and Eq. (S3)). H_2O_2 doses generated from cathodic O_2 reduction during the E-peroxone process were estimated based on H_2O_2 concentrations measured during electrolysis with pure O_2 gas sparging (see Fig. S2(d)), assuming that the presence of O_3 does not considerably influence H_2O_2 production from cathodic O_2 reduction during the E-peroxone process (Xia et al., 2017). The molar ratio of O_3:H_2O_2 during the E-peroxone process is then calculated based on the amounts of consumed O_3 doses and electro-generated H_2O_2 doses and shown in Fig. S2(e). Due to the change in O_3 consumption rate during the treatment, the ratio of O_3:H_2O_2 decreased from ~1.7 to ~0.6 in the first 5 min, then stabilized at ~0.5 afterward. These ratios are generally within the range of

O_3:H_2O_2 ratio often applied in wastewater treatment (e.g., O_3:H_2O_2 = ~0.5–2) (Bourgin et al., 2017; Soltermann et al., 2017).

$$C_{O3,consumed} = \frac{Q_{O3} \int (C_{O3,inlet} - C_{O3,outlet})\, dt}{V} - C_{O3,aqueous} \quad \text{(S3)}$$

where $C_{O3,consumed}$ is the consumed O_3 dose (mg/L), $C_{O3,inlet}$ and $C_{O3,outlet}$ are gaseous O_3 concentration at the reactor inlet and outlet, respectively (mg/L), Q_{O3} is the flow rate of sparged gas (L/min), t is the reaction time (min), V is the solution volume (L), and $C_{O3,aqueous}$ is the aqueous O_3 concentration during the treatment (mg/L).

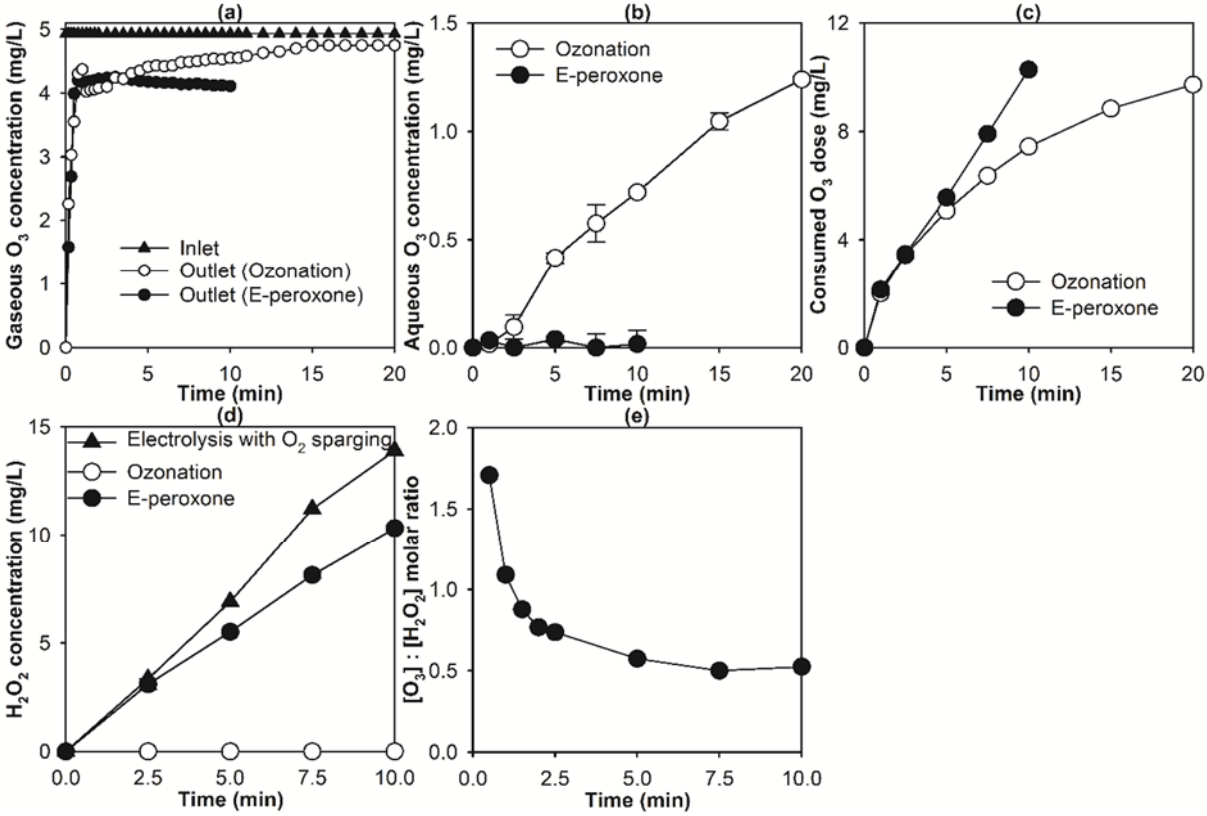

Fig. S2 (a) Gaseous O_3 concentration, (b) aqueous O_3 concentration, (c) consumed O_3 dose, (d) H_2O_2 concentration, and (e) molar ratio of aqueous O_3 to H_2O_2 during ozonation and E-peroxone treatment of the secondary effluent wastewater. (Reaction conditions: concentration of each pharmaceutical ~1 μg/L, volume = 250 mL, current = 35 mA, Pt anode = 2 × 2 cm^2, carbon-PTFE cathode = 5 × 2 cm^2, O_3 concentration = 4.8 mg/L, O_3 gas flow rate = 0.35 L/min, temperature = 15℃)

S2.2 QSAR model development for ozone rate constant (k_{O3}) estimation

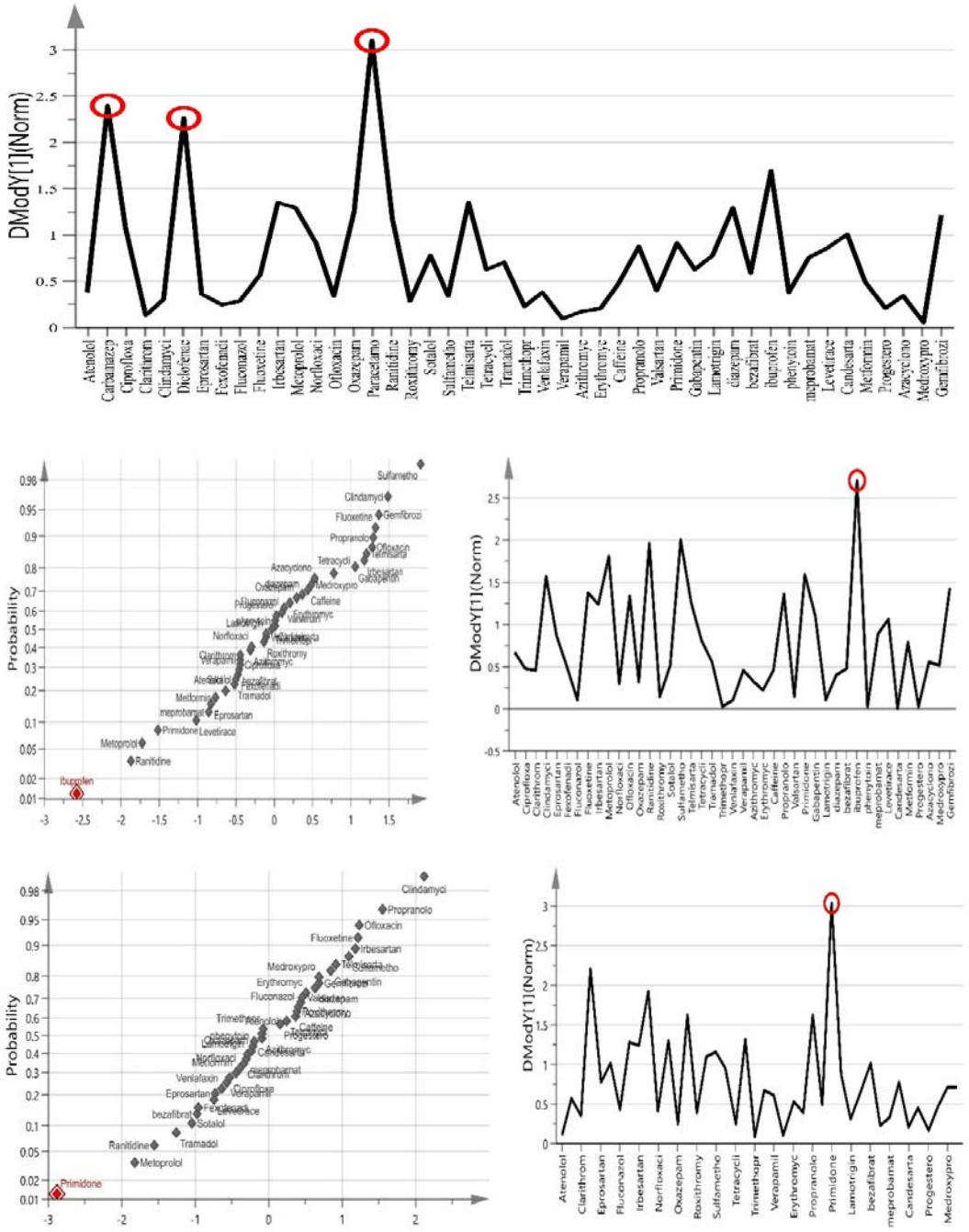

Fig. S3 Outliers (paracetamol, carbamazepine, diclofenac, ibuprofen, and primidone) identified in DModY and Normal probability graphs during development of the QSAR model developed to predict second order rate constants of pharmaceuticals' reactions with ozone (k_{O3})

Table S5 Parameters of the QSAR model developed to predict second order rate constants of pharmaceuticals' reactions with ozone (k_{O3}), based on data for 40 pharmaceuticals and a final set of 44 descriptors after removing non-significant descriptors and outliers

Component	R^2X	R^2X (cum)	Eigenvalue	R^2	R^2 (cum)	Q^2	Limit	Q^2 (cum)	R^2Y (cum)
Model		0.34			0.96			0.84	1
Predictive		0.15			0.96			0.84	1
P1	0.15	0.15	6.11	0.96	0.96	0.84	0.01	0.84	1
Orthogonal in X (OPLS)		0.15			0				
O1	0.12	0.12	4.82	0	0				
O2	0.08	0.19	3.07	0	0				

Table S6 List of descriptors (and their sources) used to develop the QSAR model after removing non-significant descriptors

Descriptor	Explanation	Source
AM1_HOMO	HOMO energy (eV)	MOE
AM1_LUMO	LUMO energy (eV)	MOE
ASA +	Positive accessible surface area	MOE
a_nS	Number of sulfur atoms	MOE
balabanJ	Balaban averaged distance sum connectivity	MOE
DASA	Absolute difference in surface area	MOE
Diameter	Largest vertex eccentricity in graph	MOE
Dipole	Dipole moment	MOE
Glob	Molecular globularity	MOE
Q_RPC +	Relative positive partial charge	MOE
Q_VSA_FPPOS	Fractional polar positive vdw surface area	MOE
Std_dim1	Standard dimension 1	MOE
VDistEq	Vertex distance equality index	MOE
N%	Percentage of N atoms	DRAGON
O%	Percentage of O atoms	DRAGON
nR07	Number of 7-membered rings	DRAGON
nCrq	Number of ring quaternary C (sp3)	DRAGON
nRCONR2	Number of tertiary amides (aliphatic)	DRAGON
nROCON	Number of (thio-) carbamates (aliphatic)	DRAGON
nArCO	Number of ketones (aromatic)	DRAGON
nC(= N)N2	Number of guanidine derivatives	DRAGON
nArC = N	Number of imines (aromatic)	DRAGON
nRNR2	Number of tertiary amines (aliphatic)	DRAGON
nArOH	Number of aromatic hydroxyls	DRAGON
nArOR	Number of ethers (aromatic)	DRAGON
nRSR	Number of sulfides	DRAGON
nArX	Number of X on aromatic ring	DRAGON

nTriazoles	Number of triazoles	DRAGON
C-005	CH3X	DRAGON
C-019	= CRX	DRAGON
C-026	R–CX–R	DRAGON
C-027	R–CH–X	DRAGON
C-030	X–CH–X	DRAGON
C-031	X–CR–X	DRAGON
C-034	R–CR..X	DRAGON
C-041	X-C(= X)-X	DRAGON
H-047	H attached to C1(sp3)/C0(sp2)	DRAGON
O-057	Phenol / enol / carboxyl OH	DRAGON
O-060	Al-O-Ar /Ar-O-Ar / R..O..R / R-O-C = X	DRAGON
N-068	Al3-N	DRAGON
N-072	RCO-*N* < / > N-X = X	DRAGON
N-074	R#N / R = N-	DRAGON
Cl-089	Cl attached to C1(sp2)	DRAGON
S-107	R2S / RS-RS	DRAGON

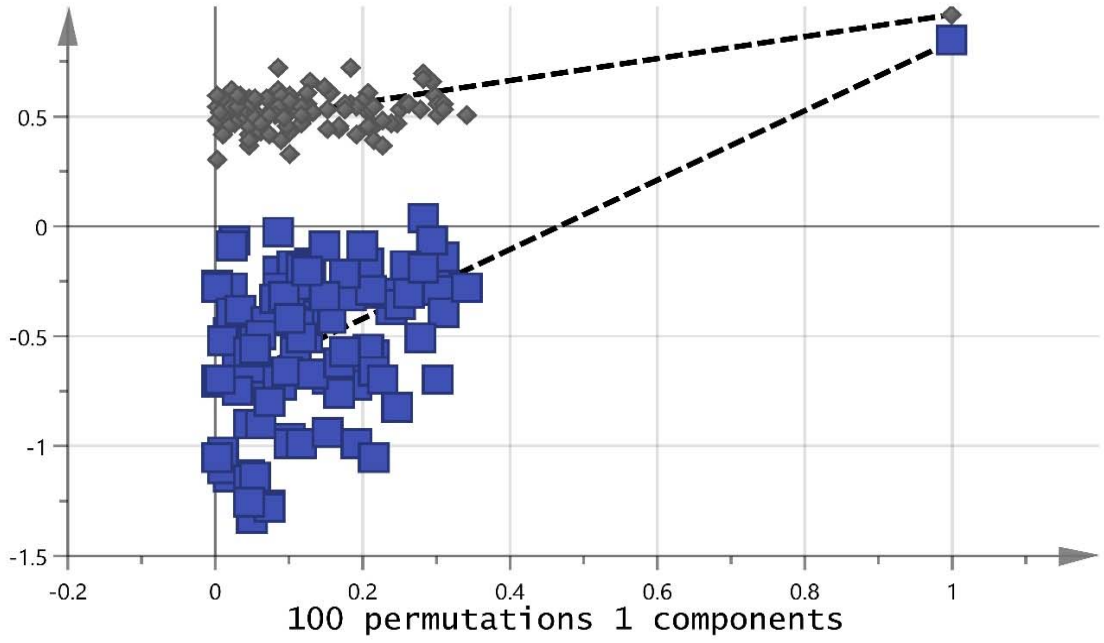

Fig. S4 Permutation plot showing the apparent lack of random collinearity in the data set (for 40 pharmaceuticals and a final set of 44 descriptors after removing non-significant descriptors and outliers) used to construct the QSAR model to predict second order rate constants of pharmaceuticals' reactions with ozone (k_{O3})

S2.3 Energy consumption

Based on consumed ozone doses and electrical energy for H_2O_2 electro-generation, the energy consumption (EC, kWh) as a function of the treatment time of conventional ozonation and the E-peroxone process is calculated using Eqs. (S4) and (S5) and shown in Fig. S5.

$$EC_{Ozonation} = r\, C_{O3,consumed}\, V \times 10^{-6} \quad , \qquad (S4)$$

$$EC_{E\text{-}peroxone} = [r\, C_{O3,consumed}\, V + 16.7\, U\, I\, t] \times 10^{-6} \quad , \qquad (S5)$$

where r is the energy requirement for O_3 production (15 kWh/kg O_3) (Rosenfeldt et al., 2006), $C_{O3,consumed}$ is the consumed O_3 dose (mg/L), V is the solution volume (L), t is the reaction time (min), I is the applied current (A), and U is the average cell voltage (V).

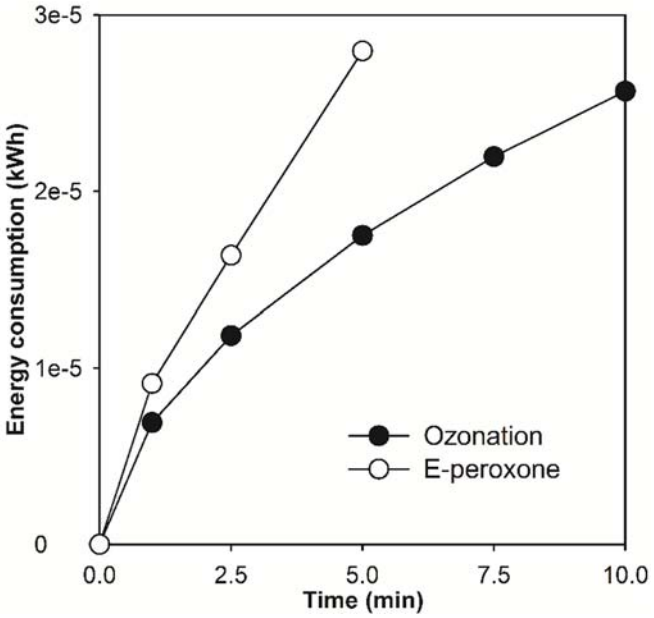

Fig. S5 Energy consumption of pharmaceutical abatements during ozonation and the E-peroxone process. (Reaction conditions were the same as that in Fig. S2)

For the same treatment time, the E-peroxone process consumed ~24%–37% more energy than conventional ozonation because of the extra energy demand for H_2O_2 electro-generation. However, due to the enhanced •OH production from O_3 decomposition by electro-generated H_2O_2, the E-peroxone process can reduce the ozone doses required to eliminate micropollutants compared to conventional ozonation (Yao et al., 2018). As a result, the E-peroxone process usually will not considerably increase, or can even reduce the energy consumption for micropollutant abatement during water and wastewater treatment compared to conventional ozonation (Yao et al., 2016; Yao et al., 2018). As shown in Fig. 1, conventional ozonation and the E-peroxone process eliminated all spiked pharmaceuticals (with the only exception of fluconazole) in the selected wastewater in 10 and 5 min, when ~7.4 and 5.6 mg/L O_3 were consumed during the two processes, respectively (see SI Fig. S2(c)). Due to its lower O_3 dosage, the E-peroxone process actually consumed similar energy to abate the spiked pharmaceuticals in

the selected wastewater as conventional ozonation (~2.80×10^{-5} and 2.57×10^{-5} kWh, see Fig. S5), despite its extra energy demand for H_2O_2 electro-generation.

S2.4 Pharmaceutical abatement as a function of consumed O_3 dose

Figure S6 shows the abatement efficiency of pharmaceuticals as a function of consumed O_3 dose during conventional ozonation and the E-peroxone treatment. As can be seen, the consumed O_3 doses to abate pharmaceuticals to a certain efficiency increased with the decrease of their ozone reactivity. For the ozone-reactive and moderately ozone-reactive species, very similar O_3 doses were consumed during ozonation and E-peroxone processes (Figs. S6(a)–S6(c)). However, for the ozone-refractory pharmaceuticals, higher abatement efficiencies were obtained at a given consumed ozone dose during the E-peroxone process than during conventional ozonation (Figs. S6(d)–S6(f)). These observations are consistent with the findings of previous studies on the E-peroxone process and can be attributed to the higher •OH yield from H_2O_2-induced O_3 decomposition than that from natural O_3 decomposition (von Sonntag and von Gunten, 2012; Yao et al., 2017; Wang et al., 2018). Due to the enhanced •OH production, lower ozone doses are required to abate ozone-refractory pharmaceuticals during the E-peroxone process than during conventional ozonation (Yao et al., 2017; Yao et al., 2018).

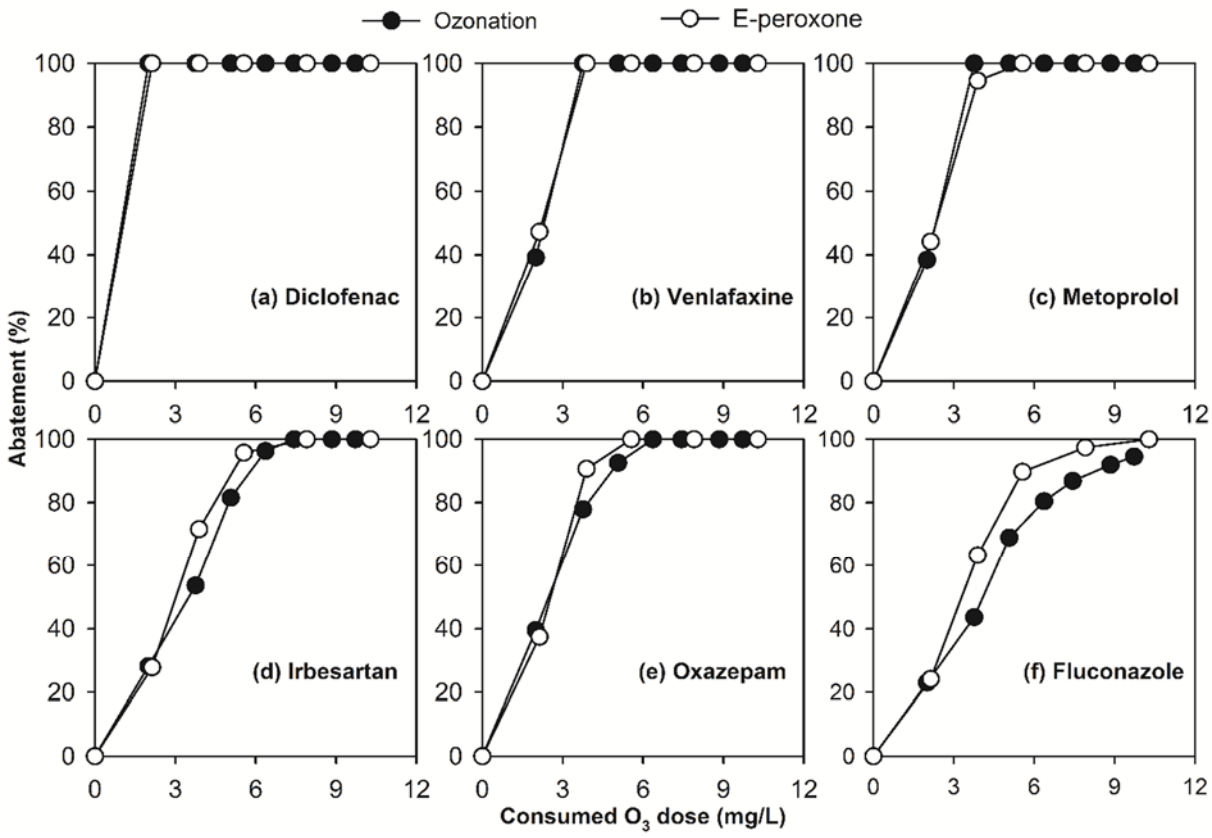

Fig. S6 Pharmaceutical abatement as a function of the consumed O_3 dose during ozonation and the E-peroxone treatment. (a) Diclofenac was selected to represent the ozone-reactive species, (b) venlafaxine and (c) metoprolol were selected to represent the moderately ozone-reactive species, and (d) irbesartan, (e) oxazepam, and (f)

fluconazole were selected to represent the ozone-refractory species. (Reaction conditions were the same as that in Fig. S2)

S2.5 O_3 and •OH exposures

To verify the enhanced •OH production from O_3 decomposition by electro-generated H_2O_2, O_3 and •OH exposures during conventional ozonation and the E-peroxone treatment of the wastewater were determined by following the evolution of aqueous O_3 and fluconazole concentrations, respectively (von Sonntag and von Gunten, 2012). Figure S2(b) shows that under the same O_2/O_3 gas sparging conditions, aqueous O_3 concentrations were considerably lower during the E-peroxone process than during conventional ozonation. Consequently, O_3 exposures increased at substantially lower rates during the E-peroxone process than during conventional ozonation (Fig. S7(a)). In contrast, •OH exposures increased much faster during the E-peroxone process than conventional ozonation (Fig. S7(b)). These observations confirm that the electro-generation of H_2O_2 considerably enhances the transformation of O_3 to •OH, thus resulting in higher •OH concentrations during the E-peroxone process than during conventional ozonation.

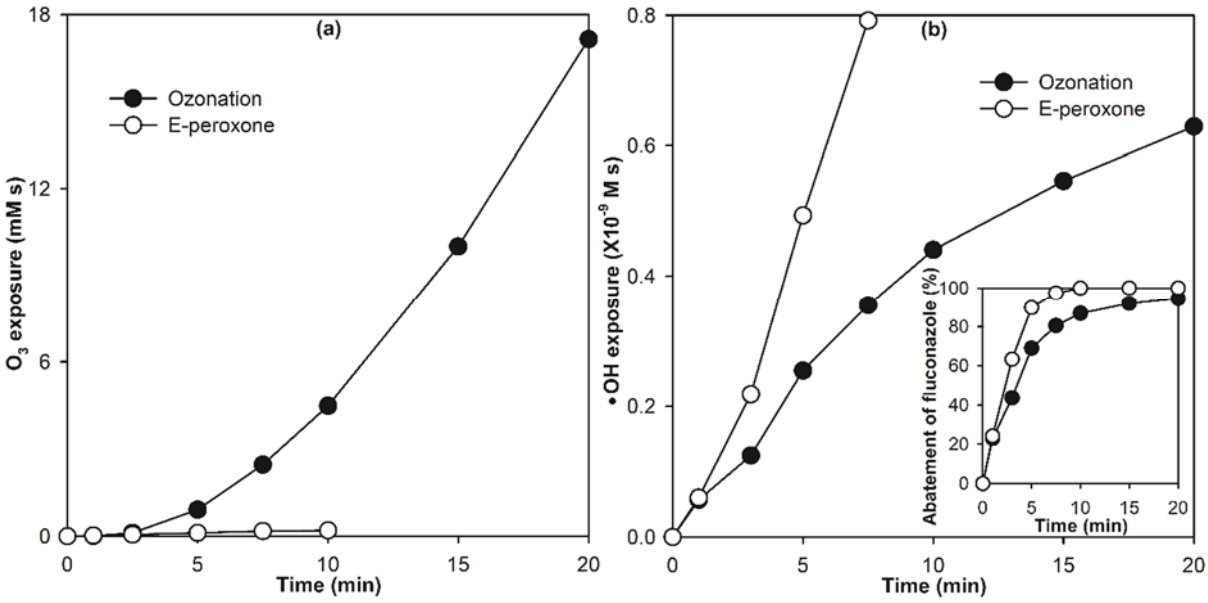

Fig. S7 Exposure to (a) O_3 and (b) •OH during ozonation and the E-peroxone treatment. The inset plot of Fig. S7(b) shows abatement of fluconazole during both treatments. (Reaction conditions were the same as that in Fig. S2)

S2.6 Kinetics of pharmaceutical abatement by conventional ozonation and E-peroxone

Figure S8 shows that of the 43 pharmaceuticals for which k_{OZ} and k_{EP} values could be calculated, 29 pharmaceuticals have a larger k_{EP} than k_{OZ} ($k_{EP}/k_{OZ} > 1$), while 14 pharmaceuticals have a smaller k_{EP} than k_{OZ} ($k_{EP}/k_{OZ} < 1$). This observation suggests that the change of conventional ozonation to E-peroxone may have different effects on the abatement of pharmaceuticals with different ozone reactivities (see Figs. 1 and 4 in the main paper for more discussion).

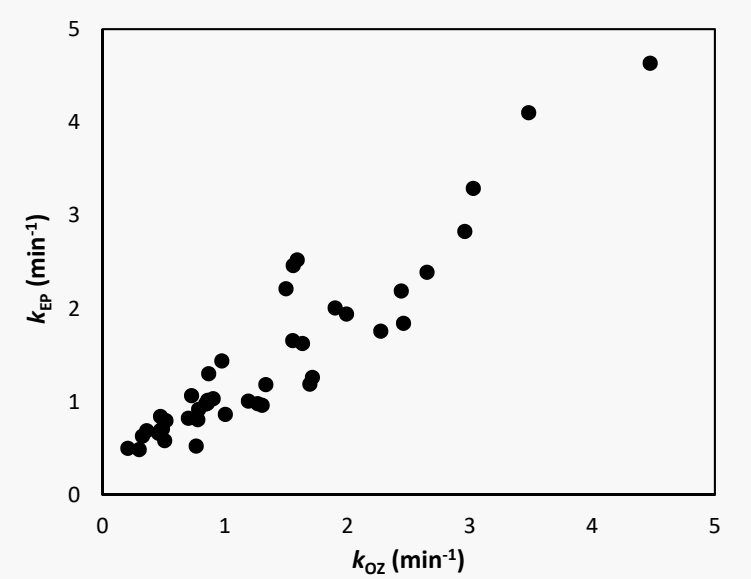

Fig. S8 Relationship between the pseudo-first order rate constant of E-peroxone (k_{EP}) and ozonation (k_{OZ}) for abatement of 43 pharmaceuticals

S2.7 Relationship between literature reported k_{O3} and experimentally measured k_{EP}/k_{OZ}

Figure S9 shows the ratio of k_{EP}/k_{OZ} of pharmaceuticals as a function of their literature-reported O_3 rate constant (k_{O3}). Note that the O_3 rate constants (k_{O3}) of most pharmaceuticals tested in this study are still unknown. Therefore, only 17 pharmaceuticals that have literature-reported k_{O3} are plotted in the figure. Overall, two general trends are observed in Fig. S9. In the $10^{-1} \leq k_{O3} \leq 10^4$ $M^{-1}\cdot s^{-1}$ range, the k_{EP}/k_{OZ} ratio decreases logarithmically from ~2.1 to 1.0 as the pharmaceuticals' k_{O3} increases ($R^2 = 0.631$). In contrast, the k_{EP}/k_{OZ} ratio for most ozone-reactive pharmaceuticals (with $k_{O3} > 10^4$ $M^{-1}\cdot s^{-1}$) is generally close to 1.

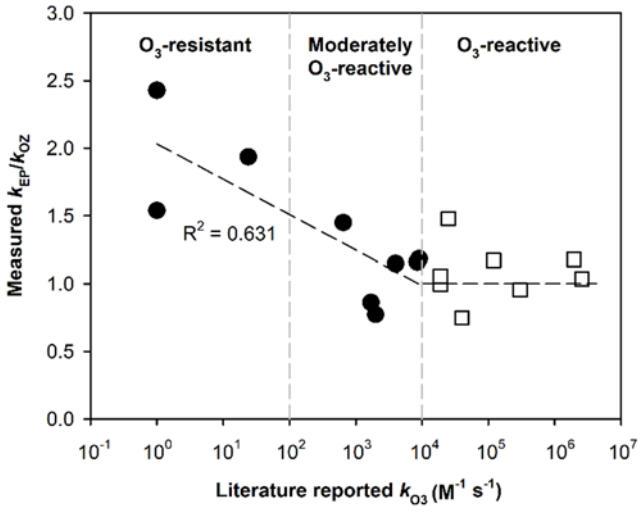

Fig. S9 The ratio of pseudo-first order rate constants for pharmaceuticals' abatement during the E-peroxone and ozonation treatments (k_{EP}/k_{OZ}) as a function of literature reported second-order rate constants for their reactions with ozone (k_{O3})

The trends shown in Fig. S9 suggest that changing from ozonation to the E-peroxone process can substantially accelerate the abatement of pharmaceuticals with low ozone reactivity (k_{EP}/k_{OZ} = ~1.5–2.5 for pharmaceuticals with $k_{O3} < 10^3$ $M^{-1}\cdot s^{-1}$). They also indicate that the shift would not substantially affect abatement of ozone-reactive pharmaceuticals (k_{EP}/k_{OZ} = ~1 for most pharmaceuticals with $k_{O3} > 10^4$ $M^{-1}\cdot s^{-1}$). The abatement of pharmaceuticals with intermediate ozone-reactivity could apparently be moderately accelerated or decelerated (k_{EP}/k_{OZ} = ~0.8–1.2 for pharmaceuticals with k_{O3} = ~10^3–10^4 $M^{-1}\cdot s^{-1}$).

S2.8 External validation and error estimation of prediction in QSAR model for ln(k_{O3})

To estimate the error in predictions by the QSAR model, a Principal Component Analysis (PCA) was developed using the same 40 pharmaceuticals and 44 descriptors (Table S7). The training set (31 pharmaceuticals) and test set (consisted of atenolol, metoprolol, norfloxacin, roxithromycin, telmisartan, venlafaxine, diazepam, phenytoin, metformin, and medroxyprogesterone) were chosen from PCA independent of k_{O3}. Further, another OPLS model was developed based solely on the training set and 44 descriptors, without the test set. The resulting model was robust with R^2 and Q^2 values of 0.97 and 0.79, respectively, and no indications of random collinearity in the model (Table S8). The developed model predicted the test set well and the error of the predictions (RMSEP) was factors of 1/3 and 3 of k_{O3} as marked by the boundary lines in Fig. S10.

Table S7 PCA model parameters based on the 40 OMPs and 44 descriptors

Component	R^2X	R^2X (cum)	Eigenvalue	Q^2	Limit	Q^2 (cum)
0	Cent.					
1	0.20	0.20	8.06	0.1	0.05	0.099
2	0.11	0.31	4.53	–0.01	0.05	0.093

Table S8 Parameters of the QSAR model based on the training set of 30 pharmaceuticals and the same 44 descriptors used for external validation and estimation of error in the predictions of ln(k_{O3}) values

Component	R^2X	R^2X (cum)	Eigenvalue	R^2	R^2 (cum)	Q^2	Limit	Q^2 (cum)	R^2Y (cum)
Model		0.34			0.97			0.79	1
Predictive		0.15			0.97			0.79	1
P1	0.15	0.15	4.51	0.97	0.97	0.79	0.01	0.79	1
Orthogonal in X (OPLS)		0.20			0				
O1	0.13	0.13	3.96	0	0				
O2	0.07	0.20	2.13	0	0				

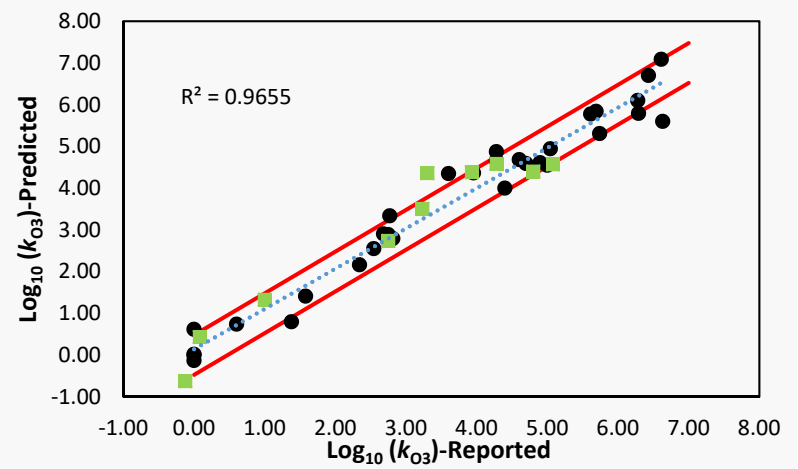

Fig. S10 Correlation between the literature-reported and QSAR model-predicted second-order rate constants for the reaction of O_3 with compounds, based on training set of 30 pharmaceuticals (circles) and test set of 10 pharmaceuticals (squares), used for external validation and estimation of error in the predictions

S2.9 Relationship between pharmaceuticals physico-chemical properties and their k_{O3}

The variable importance for the projection (VIP) plot, shown in Fig. 3 in the paper, is describing negatively and positively correlated descriptors to k_{O3}, and they are discussed separately for easiness. The most strongly negatively correlated descriptors, responsible for low O_3 reactivity, are electron withdrawing functionalities or moieties. These include: nRCONR2 (number of tertiary amides, aliphatic), N-072 (RCO-*N* < / > N-X = X), N% (percentage of nitrogen), nArC = N (number of imines, aromatic), C-041 (X-C(= X)-X), Cl^-089 (Cl attached to C1(sp2)), nArX (number of X on aromatic ring), N-074 (R#N / R = N-), n-triazoles, C-030 (X–CH–X), nROCON (number of (thio-) carbamates, aliphatic), nC(= N)N2 (number of guanidine derivatives), and C-031 (X–CR–X). These observations are consistent with previous findings (Huber et al., 2003; Jin and Peldszus, 2012; Jin et al., 2012; Sudhakaran et al., 2012; Sudhakaran and Amy, 2013; Li et al., 2019). For example, it is well-known that electron withdrawing groups or atoms can increase the ozone resistance of OMPs because they reduce the molecules' electron density and hinder electrophilic substitution reaction with O_3 (von Sonntag and von Gunten, 2012). Besides the abovementioned descriptors, nR07 (7-membered rings) and nCrq (number of ring quaternary C(sp3)) also reportedly correlate negatively with k_{O3}, putatively due to the associated lack of active sites for electrophilic ozone attack (von Sonntag and von Gunten, 2012). Some descriptors related to shape, including glob (molecular globularity) and branching and atomic connectivity (Balaban J Index, or averaged distance sum connectivity), and partial charge descriptors Q_RPC + (relative positive partial charge) and Q_VSA_FPPOS (fractional polar positive vdw surface area) are also negatively correlated with k_{O3}. Interestingly, our results suggest that pharmaceuticals with low k_{O3} tend to have relatively high lowest unoccupied molecular orbital (LUMO) energy (AM1_LUMO) values, in contrast to previous findings (Jiang et al., 2010).

The most important positively correlated descriptors, associated with high ozone reactivity of pharmaceuticals (high k_{O3}), include: the size-related variable Std_dim1 (Standard dimension 1);

highest occupied molecular orbital (HOMO) energy (AM1_HOMO); the conformation-dependent charge descriptors ASA + (positive accessible surface area) and DASA (absolute difference in surface area); adjacency and distance matrix descriptors VDisEq (vertex distance equality index) and diameter (largest vertex eccentricity in graph); and electron rich/donating moieties or functionalities, including H-047 (H attached to C1(sp3)/C0(sp2)), N-068 (Al3-N), nRNR2 (number of tertiary amines, aliphatic), O% (percentage of O atoms), a_nS (number of sulfur atoms), O-060 (Al-O-Ar /Ar-O-Ar / R..O..R / R-O-C = X), S-107 (R2S / RS-RS), nArOR (number of ethers, aromatic), nRSR (number of sulfides), O-057 (phenol/enol/carboxyl OH), nArCO (number of ketones, aromatic), and nArOH (number of aromatic hydroxyls). The identified correlations between ozone reactivity and HOMO, surface area and descriptors related to electron rich/donating functionalities are consistent with previous findings (Dodd et al., 2006; Lei and Snyder, 2007; Sudhakaran and Amy, 2013; Li et al., 2019). In addition, Std_dim1 and VDisEq descriptors are also positively correlated to ozone reactivity, either by direct effect or indirect effect, resulting from the combination of inter-correlated descriptors. Interestingly, halogens connected to aliphatic carbons (C-005 (CH3X), C-034 (R–CR..X), C-027 (R–CH–X), C-019 (= CRX), C-026 (R–CX–R)) appeared to correlate positively with ozone reactivity, in contrast to halogens connected to aromatic rings in negatively correlated descriptors.

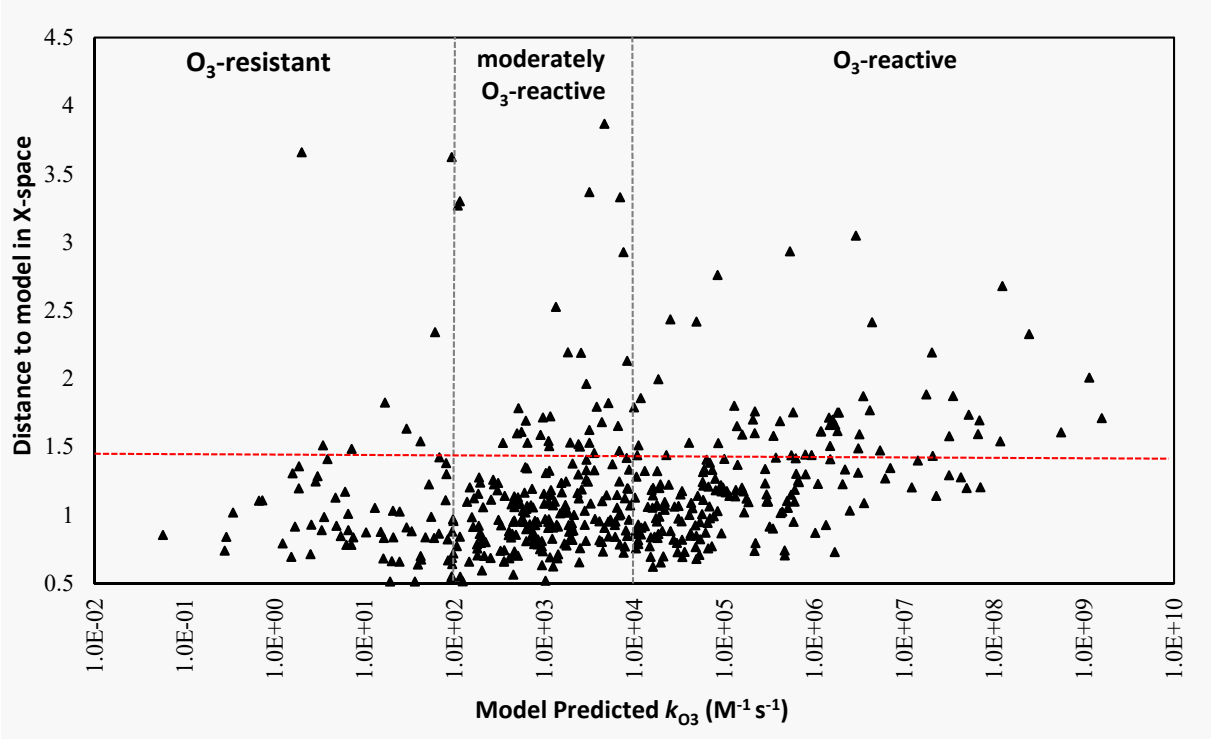

Fig. S11 QSAR model applicability domain as predicted k_{O3} of pharmaceuticals in relation to their distance to model (DmodX)

Table S9 QSAR model predicted k_{O3} of (a) O_3-resistant, (b) moderately O_3-reactive, and (c) O_3-reactive pharmaceuticals other than studied experimentally

(a)

O_3-resistant pharmaceuticals	**Predicted k_{O3} ($M^{-1}\cdot s^{-1}$)**	**O_3-resistant pharmaceuticals**	**Predicted k_{O3} ($M^{-1}\cdot s^{-1}$)**
*ciclosporin	7.49×10^{-5}	moxonidine	20.9
triazolam	0.0574	dihydralazine	24.6
lorazepam	0.28	chlordiazepoxide	29.3
clobazam	0.67	*streptomycin	29.3
anastrozole	1.23	melagatran	33.4
letrozole	1.69	pyrimethamine	36.4
*methenamine	2	ketamine	39.2
clonidine	2.52	isoflurane	41.9
carisoprodol	2.86	lomustine	42.1
amiloride	3.01	loratadine	47.6
amantadine	3.45	Dihydroergocornine	52
voriconazole	3.56	guanethidine	55
proguanil	3.88	*itraconazole	60.8
artemether	4.75	lisinopril	67.1
pentobarbital	4.88	piperacillin	68
midazolam	5.46	mercaptopurine	80.7
anagrelide	6.08	domperidone	81.5
ribavirin	6.58	flucytosine	84.2
praziquantel	6.6	efavirenz	84.9
ethosuximide	7.13	Baclofen	91
felbamate	10.4	*caspofungin	93.1
nitrazepam	13	gemcitabine	93.1
zidovudine	15.2	nortriptyline	93.8
methohexital	16.2	oxcarbazepine	94.4
*levosimendan	16.9	quinaprilate	94.4
phenobarbital	19.2	alfentanil	96.2
mitotane	20.7	loracarbef	96.9

(b)

Moderately O_3-reactive pharmaceuticals	**Predicted k_{O3} ($M^{-1}\cdot s^{-1}$)**	**Moderately O_3-reactive pharmaceuticals**	**Predicted k_{O3} ($M^{-1}\cdot s^{-1}$)**	**Moderately O_3-reactive pharmaceuticals**	**Predicted k_{O3} ($M^{-1}\cdot s^{-1}$)**
ramiprilate	1.06×10^2	chlorzoxazone	6.32×10^2	ropivacaine	2.02×10^3
*deferoxamine	1.09×10^2	lopinavir	6.43×10^2	amikacin	2.06×10^3
*pancuroniumbromide	1.15×10^2	pirenzepine	6.47×10^2	bupivacaine	2.10×10^3
zalcitabine	1.16×10^2	tenofovir	6.89×10^2	ezetimibe	2.13×10^3
stavudine	1.23×10^2	trimipramine	7.08×10^2	dantrolene	2.38×10^3
amfetamine	1.46×10^2	pentoxifylline	7.13×10^2	docetaxel	2.39×10^3
thiopental	1.56×10^2	thiamazole	7.29×10^2	netilmicin	2.41×10^3

cyproterone	1.61×10^2	prednisone	7.36×10^2	metoclopramide	2.44×10^3
enalaprilate	1.78×10^2	imipramine	7.46×10^2	pimecrolimus	2.48×10^3
phenylpropanolamine	1.80×10^2	mefloquine	7.52×10^2	atomoxetine	2.49×10^3
vigabatrin	1.80×10^2	chlortalidone	7.67×10^2	*foscarnetsodium	2.55×10^3
ethambutol	1.84×10^2	minoxidil	7.86×10^2	zoledronicacid	2.80×10^3
Ajmaline	1.86×10^2	isoniazid	7.91×10^2	mepivacaine	2.88×10^3
pamidronicacid	1.88×10^2	chloramphenicol	8.35×10^2	aripiprazole	2.91×10^3
Aciclovir	1.91×10^2	exemestane	8.39×10^2	*glycopyrronium	2.92×10^3
trandolaprilate	1.97×10^2	hydralazine	8.48×10^2	pyrazinamide	2.93×10^3
ganciclovir	2.01×10^2	mexiletine	8.96×10^2	gentamicin C1	3.05×10^3
phenelzine	2.02×10^2	*ifosfamide	9.06×10^2	misoprostol	3.16×10^3
losartan	2.52×10^2	prilocaine	9.38×10^2	*oxytocin	3.16×10^3
tadalafil	2.69×10^2	hyoscyamine	9.57×10^2	tacrolimus	3.57×10^3
dicloxacillin	2.75×10^2	*fosfomycin	9.62×10^2	zopiclone	3.58×10^3
theophylline	3.01×10^2	selegiline	9.88×10^2	chlorambucil	3.65×10^3
doxapram	3.05×10^2	methadone	9.96×10^2	acetylsalicylicacid	4.09×10^3
levonorgestrel	3.08×10^2	felodipine	1.02×10^3	pethidine	4.09×10^3
cidofovir	3.25×10^2	methylphenidate	1.03×10^3	hydroxychloroquine	4.30×10^3
ambroxol	3.30×10^2	miglustat	1.04×10^3	*cetirizine	4.34×10^3
argatroban	3.46×10^2	acetylcysteine	1.10×10^3	rivastigmine	4.34×10^3
ephedrine	3.56×10^2	lidocaine	1.10×10^3	milrinone	4.47×10^3
pseudoephedrine	3.56×10^2	pemetrexed	1.11×10^3	*obidoxime	4.64×10^3
penciclovir	3.57×10^2	emedastine	1.12×10^3	propofol	4.64×10^3
ergotamine	3.61×10^2	megestrol	1.12×10^3	methotrexate	4.91×10^3
aceclofenac	4.01×10^2	ketoconazole	1.13×10^3	terbinafine	5.12×10^3
testosterone	4.03×10^2	propylthiouracil	1.15×10^3	*flunarizine	5.15×10^3
betamethasone	4.26×10^2	*meclozine	1.16×10^3	mifepristone	5.17×10^3
etonogestrel	4.38×10^2	mizolastine	1.18×10^3	tropisetron	5.44×10^3
cladribine	4.50×10^2	bromhexine	1.19×10^3	zolmitriptan	6.10×10^3
norethisterone	4.50×10^2	Abacavir	1.25×10^3	phenazone	6.16×10^3
nitrofurantoin	4.52×10^2	betahistine	1.25×10^3	clomethiazole	6.41×10^3
alendronicacid	4.63×10^2	flucloxacillin	1.25×10^3	metronidazole	6.42×10^3
fentanyl	4.63×10^2	*neostigmine	1.34×10^3	amlodipine	6.71×10^3
oxandrolone	4.64×10^2	modafinil	1.37×10^3	oxybutynin	6.89×10^3
oseltamivir carboxylate	4.65×10^2	remifentanil	1.39×10^3	*atosiban	6.93×10^3
nevirapine	4.81×10^2	disopyramide	1.41×10^3	pravastatin	7.01×10^3
*clozapine	4.96×10^2	Atropine	1.42×10^3	*pyridostigmine	7.56×10^3
flumazenil	5.08×10^2	ampicillin	1.50×10^3	ketoprofen	7.59×10^3
simvastatin	5.08×10^2	tobramycin	1.54×10^3	granisetron	7.84×10^3
dienogest	5.12×10^2	cloxacillin	1.61×10^3	acamprosate	7.86×10^3
*sirolimus	5.15×10^2	scopolamine	1.67×10^3	acrivastine	8.05×10^3
fosinoprilate	5.42×10^2	didanosine	1.71×10^3	meropenem	8.20×10^3
clobutinol	5.54×10^2	fluvoxamine	1.71×10^3	*everolimus	8.30×10^3

*allopurinol	5.56×10^2	levocabastine	1.74×10^3	Carteolol	8.33×10^3
moclobemide	5.67×10^2	zaleplon	1.76×10^3	reboxetine	8.36×10^3
rizatriptan	5.77×10^2	benzylpenicillin	1.83×10^3	nitisinone	8.52×10^3
solifenacin	5.96×10^2	levobupivacaine	1.88×10^3	phentolamine	8.71×10^3
saquinavir	6.13×10^2	Dextropropoxyphene	1.91×10^3	bicalutamide	8.73×10^3
*butylskopolamine	6.22×10^2	neomycinC	1.93×10^3	entacapone	8.97×10^3
prednisolone	6.28×10^2	ropinirole	1.97×10^3	*cinnarizine	9.91×10^3
captopril	6.29×10^2				

(c)

O_3-reactive pharmaceuticals	**Predicted k_{O3} ($M^{-1}\cdot s^{-1}$)**	**O_3-reactive pharmaceuticals**	**Predicted k_{O3} ($M^{-1}\cdot s^{-1}$)**	**O_3-reactive pharmaceuticals**	**Predicted k_{O3} ($M^{-1}\cdot s^{-1}$)**
Estrone	1.01×10^4	ketorolac	4.91×10^4	*lanreotide	5.36×0^5
phenoxymethylpenicillin	1.02×10^4	hydrochlorothiazide	5.06×10^4	naratriptan	5.51×10^5
phenylephrine	1.02×10^4	furosemide	5.27×10^4	apomorphine	5.56×10^5
Estradiol	1.04×10^4	tinidazole	5.37×10^4	*tirofiban	5.81×10^5
Etilefrine	1.04×10^4	tetracaine	5.39×10^4	rabeprazole	5.90×10^5
ticlopidine	1.07×10^4	droperidol	5.75×10^4	tiludronicacid	6.03×10^5
ethinylestradiol	1.10×10^4	valdecoxib	5.80×10^4	vardenafil	6.21×10^5
methylergometrine	1.10×10^4	Dapsone	5.82×10^4	methoxsalen	6.28×10^5
irinotecan	1.11×10^4	mesalazine	5.85×10^4	sumatriptan	6.61×10^5
salbutamol	1.11×10^4	aztreonam	6.36×10^4	eletriptan	6.75×10^5
indometacin	1.13×10^4	guaifenesin	6.53×10^4	dopexamine	7.94×10^5
*paclitaxel	1.18×10^4	nimodipine	6.62×10^4	amsacrine	8.03×10^5
galantamine	1.20×10^4	ziprasidone	6.84×10^4	Bosentan	9.31×10^5
fenofibrate	1.30×10^4	indinavir	6.92×10^4	sildenafil	1.10×10^6
topiramate	1.31×10^4	oxycodone	6.92×10^4	*ceftibuten	1.18×10^6
ketobemidone	1.41×10^4	quinidine	7.26×10^4	*chlorpromazine	1.19×10^6
betaxolol	1.55×10^4	norepinephrine	7.35×10^4	piroxicam	1.35×10^6
labetalol	1.61×10^4	yohimbine	7.62×10^4	*quetiapine	1.46×10^6
leflunomide	1.61×10^4	buspirone	7.90×10^4	carvedilol	1.50×10^6
warfarin	1.68×10^4	liothyronine	8.02×10^4	almotriptan	1.51×10^6
pentazocine	1.74×10^4	topotecan	8.40×10^4	*doxycycline	1.81×10^6
melperone	1.78×10^4	*quinupristin	8.43×10^4	*cefotaxime	1.81×10^6
nicotinicacid	1.78×10^4	deferiprone	8.54×10^4	*zuklopenthixol	1.88×10^6
cimetidine	1.79×10^4	etoricoxib	9.17×10^4	nedocromil	2.07×10^6
amoxicillin	1.81×10^4	Articaine	9.29×10^4	fenoterol	2.19×10^6
diflunisal	1.81×10^4	morphine	9.66×10^4	omeprazole	2.48×10^6
*mupirocin	1.84×10^4	acetazolamide	9.99×10^4	*vancomycin	2.90×10^6
Estriol	1.85×10^4	naltrexone	1.04×10^5	dobutamine	3.07×10^6
pindolol	1.89×10^4	hydromorphone	1.07×10^5	vinorelbine	3.08×10^6
terazosin	1.89×10^4	*ivermectin	1.29×10^5	*alimemazine	3.18×10^6
azathioprine	1.95×10^4	ketotifen	1.32×10^5	*prochlorperazine	3.50×10^6

physostigmine	1.96×10^4	*salmeterol	1.38×10^5	*famotidine	4.39×10^6
mebendazole	2.04×10^4	rofecoxib	1.41×10^5	imatinib	5.39×10^6
imipenem	2.18×10^4	timolol	1.64×10^5	nelfinavir	6.15×10^6
isradipine	2.18×10^4	isoprenaline	1.76×10^5	papaverine	7.00×10^6
cefuroxime	2.27×10^4	rosiglitazone	1.86×10^5	pantoprazole	1.21×10^7
spironolactone	2.41×10^4	*busulfan	2.08×10^5	idarubicin	1.42×10^7
*digitoxin	2.51×10^4	moxifloxacin	2.17×10^5	*cefepime	2.03×10^7
lamivudine	2.52×10^4	*doxazosin	2.18×10^5	*doxorubicin	3.16×10^7
naproxen	2.73×10^4	*olanzapine	2.19×10^5	propiomazine	3.16×10^7
pramipexole	2.79×10^4	ondansetron	2.23×10^5	lornoxicam	4.27×10^7
fluvastatin	2.98×10^4	Bendroflumethiazide	2.84×10^5	meloxicam	4.94×10^7
nabumetone	3.09×10^4	sultiame	2.84×10^5	*dixyrazine	5.21×10^7
propafenone	3.10×10^4	carebastine	2.95×10^5	*etoposide	6.61×10^7
probenecid	3.25×10^4	lansoprazole	3.01×10^5	*mitoxantrone	6.86×10^7
atovaquone	3.34×10^4	riluzole	3.06×10^5	tenoxicam	7.02×10^7
nifedipine	3.38×10^4	sulpiride	3.18×10^5	epirubicin	1.17×10^8
torasemide	3.39×10^4	bumetanide	3.47×10^5	*ceftriaxone	1.23×10^8
remoxipride	3.61×10^4	*chlorprothixene	3.52×10^5	*ceftazidime	2.44×10^8
levothyroxine	4.06×10^4	telithromycin	3.74×10^5	*nizatidine	5.55×10^8
cisapride	4.09×10^4	*chlortetracycline	4.15×10^5	*thioridazine	1.14×10^9
sufentanil	4.28×10^4	cefadroxil	4.23×10^5	*rifampicin	1.57×10^9
celecoxib	4.42×10^4	levofloxacin	4.71×10^5	*cisatracuriumbesylate	1.91×10^{11}
*digoxin	4.89×10^4	griseofulvin	4.99×10^5		

Notes: *Pharmaceuticals with distance to model larger than 1.5 (that is the limit of model applicability domain)

References

Bader H, Hoigne J (1981). Determination of ozone in water by the indigo method. Water Research, 15(4): 449–456

Borowska E, Bourgin M, Hollender J, Kienle C, Mcardell C S, von Gunten U (2016). Oxidation of cetirizine, fexofenadine and hydrochlorothiazide during ozonation: Kinetics and formation of transformation products. Water Research, 94: 350–362

Bourgin M, Beck B, Boehler M, Borowska E, Fleiner J, Salhi E, Teichler R, von Gunten U, Siegrist H, Mcardell C S (2018). Evaluation of a full-scale wastewater treatment plant upgraded with ozonation and biological post-treatments: Abatement of micropollutants, formation of transformation products and oxidation by-products. Water Research, 129: 486–498

Bourgin M, Borowska E, Helbing J, Hollender J, Kaiser H P, Kienle C, Mcardell C S, Simon E, von Gunten U (2017). Effect of operational and water quality parameters on conventional ozonation and the advanced oxidation process O_3/H_2O_2: Kinetics of micropollutant abatement, transformation product and bromate formation in a surface water. Water Research, 122: 234–245

Broséus R, Vincent S, Aboulfadl K, Daneshvar A, Sauvé S, Barbeau B, Prévost M (2009). Ozone oxidation of pharmaceuticals, endocrine disruptors and pesticides during drinking water treatment. Water Research, 43(18): 4707–4717

Buxton G V, Greenstock C L, Helman W P, Ross A B (1988). Critical review of rate constants for reactions of hydrated electrons, hydrogen atoms and hydroxyl radicals (·OH/·O⁻) in aqueous solution. Journal of Physical and Chemical Reference Data, 17(2): 677–685

Dodd M C, Buffle M O, von Gunten U (2006). Oxidation of antibacterial molecules by aqueous ozone: Moiety-specific reaction kinetics and application to ozone-based wastewater treatment. Environmental Science & Technology, 40(6): 1969–1977

Grabic R, Fick J, Lindberg R H, Fedorova G, Tysklind M (2012). Multi-residue method for trace level determination of pharmaceuticals in environmental samples using liquid chromatography coupled to triple quadrupole mass spectrometry. Talanta, 100: 183–195

Huber M M, Canonica S, Park G Y, von Gunten U (2003). Oxidation of pharmaceuticals during ozonation and advanced oxidation processes. Environmental Science & Technology, 37(5): 1016–1024

Jiang J L, Yue X A, Chen Q F, Gao Z (2010). Determination of ozonization reaction rate constants of aromatic pollutants and QSAR study. Bulletin of Environmental Contamination and Toxicology, 85(6): 568–572

Jin X, Peldszus S (2012). Selection of representative emerging micropollutants for drinking water treatment studies: A systematic approach. Science of the Total Environment, 414: 653–663

Jin X, Peldszus S, Huck P M (2012). Reaction kinetics of selected micropollutants in ozonation and advanced oxidation processes. Water Research, 46(19): 6519–6530

Keen O S, Ferrer I, Michael Thurman E, Linden K G (2014). Degradation pathways of lamotrigine under advanced treatment by direct UV photolysis, hydroxyl radicals, and ozone. Chemosphere, 117: 316–323

Lee Y, Gerrity D, Lee M, Bogeat A E, Salhi E, Gamage S, Trenholm R A, Wert E C, Snyder S A, von Gunten U (2013). Prediction of micropollutant elimination during ozonation of municipal wastewater effluents: Use of kinetic and water specific information. Environmental Science & Technology, 47(11): 5872–5881

Lee Y, Kovalova L, Mcardell C S, von Gunten U (2014). Prediction of micropollutant elimination during ozonation of a hospital wastewater effluent. Water Research, 64(0): 134–148

Lee Y, von Gunten U (2012). Quantitative structure-activity relationships (QSARs) for the transformation of organic micropollutants during oxidative water treatment. Water Research, 46(19): 6177–6195

Lei H, Snyder S A (2007). 3D QSPR models for the removal of trace organic contaminants by ozone and free chlorine. Water Research, 41(18): 4051–4060

Li X, Wang B, Wang Y, Li K, Yu G (2019). Synergy effect of E-peroxone process in the degradation of structurally diverse pharmaceuticals: A QSAR analysis. Chemical Engineering Journal, 360: 1111–1118

Lindberg R H, Ostman M, Olofsson U, Grabic R, Fick J (2014). Occurrence and behaviour of 105 active pharmaceutical ingredients in sewage waters of a municipal sewer collection system. Water Research, 58: 221–229

Muñoz I, Jose Gomez M, Molina-Diaz A, Huijbregts M A, Fernandez-Alba A R, Garcia-Calvo E (2008). Ranking potential impacts of priority and emerging pollutants in urban wastewater through life cycle impact assessment. Chemosphere, 74(1): 37–44

Rosal R, Rodríguez A, Perdigón-Melón J A, Mezcua M, Hernando M D, Letón P, García-Calvo E, Agüera A, Fernández-Alba A R (2008). Removal of pharmaceuticals and kinetics of mineralization by O_3/H_2O_2 in a biotreated municipal wastewater. Water Research, 42(14): 3719–3728

Rosenfeldt E J, Linden K G, Canonica S, von Gunten U (2006). Comparison of the efficiency of OH radical formation during ozonation and the advanced oxidation processes O_3/H_2O_2 and UV/H_2O_2. Water Research, 40(20): 3695–3704

Sellers R M (1980). Spectrophotometric determination of hydrogen peroxide using potassium titanium(IV) oxalate. Analyst (London), 105(1255): 950–954

Soltermann F, Abegglen C, Tschui M, Stahel S, von Gunten U (2017). Options and limitations for bromate control during ozonation of wastewater. Water Research, 116: 76–85

Sudhakaran S, Amy G L (2013). QSAR models for oxidation of organic micropollutants in water based on ozone and hydroxyl radical rate constants and their chemical classification. Water Research, 47(3): 1111–1122

Sudhakaran S, Calvin J, Amy G L (2012). QSAR models for the removal of organic micropollutants in four different river water matrices. Chemosphere, 87(2): 144–150

von Sonntag C, von Gunten U (2012). Chemistry of ozone in water and wastewater treatment: From basic principles to applications. London: IWA Publishing

Wang H, Zhan J, Yao W, Wang B, Deng S, Huang J, Yu G, Wang Y (2018). Comparison of pharmaceutical abatement in various water matrices by conventional ozonation, peroxone (O_3/H_2O_2), and an electro-peroxone process. Water Research, 130: 127–138

Wang Y J, Li X Y, Zhen L M, Zhang H Q, Zhang Y, Wang C W (2012). Electro-Fenton treatment of concentrates generated in nanofiltration of biologically pretreated landfill leachate. Journal of Hazardous Materials, 229–230: 115–121

Xia G, Wang Y, Wang B, Huang J, Deng S, Yu G (2017). The competition between cathodic oxygen and ozone reduction and its role in dictating the reaction mechanisms of an electro-peroxone process. Water Research, 118: 26–38

Yao W, Qu Q, von Gunten U, Chen C, Yu G, Wang Y (2017). Comparison of methylisoborneol and geosmin abatement in surface water by conventional ozonation and an electro-peroxone process. Water Research, 108: 373–382

Yao W, Ur Rehman S W, Wang H, Yang H, Yu G, Wang Y (2018). Pilot-scale evaluation of micropollutant abatements by conventional ozonation, UV/O_3, and an electro-peroxone process. Water Research, 138: 106–117

Yao W, Wang X, Yang H, Yu G, Deng S, Huang J, Wang B, Wang Y (2016). Removal of pharmaceuticals from secondary effluents by an electro-peroxone process. Water Research, 88: 826–835

Yuan S, Li Z X, Wang Y J (2013). Effective degradation of methylene blue by a novel electrochemically driven process. Electrochemistry Communications, 29: 48–51